ANALYSIS OF THE TOOL PLUNGE IN FRICTION STIR WELDING
Comparison of Aluminum Alloys 2024 T3 and 2024 T351

by

Darko M. VELJIĆ[a*], Bojan L. MEDJO[b] , Marko P. RAKIN[b], Zoran M. RADOSAVLJEVIĆ[c], and Nikola S. BAJIĆ[a]

[a] IHIS Techno Experts Research & Development Center, IHIS Science & Technology Park, Belgrade, Serbia
[b] Faculty of Technology and Metallurgy, University of Belgrade, Belgrade, Serbia
[c] Euro-Mont-Ing, Belgrade, Serbia

Original scientific paper
DOI: 10.2298/TSCI150313059V

Temperature, plastic strain and heat generation during the plunge stage of the friction stir welding of high-strength aluminum alloys 2024 T3 and 2024 T351 are considered in this work. The plunging of the tool into the material is done at different rotating speeds. A 3-D finite element model for thermomechanical simulation is developed. It is based on arbitrary Lagrangian-Eulerian formulation, and Johnson-Cook material law is used for modelling of material behaviour. From comparison of the numerical results for alloys 2024 T3 and 2024 T351, it can be seen that the former has more intensive heat generation from the plastic deformation, due to its higher strength. Friction heat generation is only slightly different for the two alloys. Therefore, temperatures in the working plate are higher in the alloy 2024 T3 for the same parameters of the plunge stage. Equivalent plastic strain is higher for 2024 T351 alloy, and the highest values are determined under the tool shoulder and around the tool pin. For the alloy 2024 T3, equivalent plastic strain is the highest in the influence zone of the tool pin.

Key words: *friction stir welding, numerical simulation, temperature fields, heat generation, equivalent plastic strain*

Introduction

Friction stir welding (FSW) is a complex and non-linear process, accompanied with large plastic strain, high temperatures and plastic flow of the material in the welding zone. Due to the complex thermo-mechanical conditions, this zone is often referred to as thermo-mechanically affected zone or thermo-mechanically affected zone. It is mostly in plastic state and it is difficult to determine its temperature, due to the large plastic strain values. The FSW process has been considered in [1-16], from the point of view of manufacturing, modelling, as well as testing of the specimens cut from the welded joints. Zhang and Zhang [1] carried out semi-coupled thermomechanical finite element (FE) analyses of the FSW process and the associated microstructural changes. In some references, the main objective was to examine the effect of various FSW process parameters (including tool design) on the heat/mass transport processes, *e. g.* [1-4]. Song and Kovačević [5] and Chen and Kovačević [6] presented numerical thermomechanical modeling of FSW for both similar and dissimilar joints; dissimilar joints

* Corresponding author; e-mail: veljic.darko@gmail.com

were also analysed in [7]. Some simplified analyses are conducted in the literature, such as Dong *et al.* [8], where several models were developed to separately deal with the thermal and mechanical aspects of the FSW. A comprehensive review of numerical analysis in the field of FSW is presented in [9].

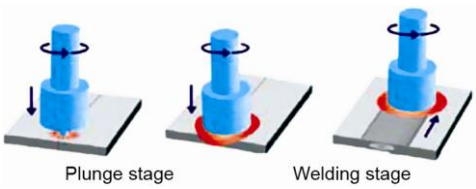

Figure 1. FSW process

The FSW process can be divided into two stages: tool plunging and linear welding, fig. 1. In majority of the literature, the emphasis is on the simulation of the welding process, *i. e.* the linear welding phase, while the plunge stage is more rarely examined. However, thermo-mechanical analysis of the tool plunging into the working plates is very important for analysis of the FSW process in general. During this stage, extremely high strains emerge in the welding zone, and the temperature reaches the value corresponding to hot plastic processing (which is approximately 80% of the melting temperature). Also, the thermomechanical conditions initiated in this stage are present during the entire welding process. Numerical modeling of the plunging process is very demanding due to the pronounced mesh distortion under the pin.

In order to analyse the plunge stage, a coupled thermo-mechanical model is developed to determine the temperature, plastic strain and generated heat for high-strength alloys Al 2024 T3 and Al 2024 T351 at different tool rotation speeds. Although, they will be referred to as two alloys in the remainder of the paper, this is actually the same Al alloy subjected to different thermal treatments and therefore denoted by different temper designations. The T3 stands for solution heat treated and then cold worked, while T351 stands for solution heat treatment and stress relief by stretching.

Material properties

In this work, the plunge stage of FSW is analysed on aluminum alloys EN AW 2024 T3 and EN AW 2024 T351. They both have the same chemical composition: Al – balance, Cu – 4.52, Mg – 1.60, Mn – 0.65, Fe – 0.28, Si – 0.12, Zn – 0.09, Ti – 0.16, Cr – 0.01, other, total – 0.02 % [5, 6], but are structurally different due to different processing procedure. In tab. 1, tensile properties of both alloys are given. The alloy 2024 T351 has lower yield strength and ultimate tensile strength than the alloy 2024 T3. Coefficients of the *Johnson Cook material model* show significantly more pronounced plasticity of 2024 T351 alloy. As the FSW process can be regarded as a method of plastic processing, it is interesting to compare the simulation results for these two alloys, in terms of temperature change, plastic strain, as well as heat generation due to friction and plastic deformation. Other material properties used in this model are given in tab. 2.

Table 1. Tensile properties of aluminum alloy 2024 [17]

Alloy	0.2% yield strength $R_{p0.2}$, [MPa]	Tensile strength R_m, [MPa]	Elongation at fracture A_5, [%]
2024 T3	345	483	18
2024 T351	324	469	20

Numerical model

Numerical simulations can be useful for development and optimization of any welding process, *e. g.* [19-21]. Of course, in addition to the simulation of the process itself, numer-

ical methods are also applied in determining the fracture behavior of the welded structures, [22].

The dimensions of the welding plate model used in this work are 50 × 50 × 3 mm; the model can be seen in figs. 2 and 3. The model consists of hexahedral elements with 8-nodes, with trilinear displacement and temperature degrees of freedom, [23]. This element is denoted in Abaqus software package as C3D8RT, has uniform strain and hourglass control [23-26].

Table 2. Material properties of Al alloy 2024 [11, 17, 18]

Material properties	Value
Young's modulus of elasticity, [GPa]	73.1
Poisson´s ratio, [–]	0.33
Thermal conductivity, [$Wm^{-1}°C^{-1}$]	121
Coefficient of thermal expansion, [$°C^{-1}$]	$24.7 \cdot 10^{-6}$
Density, [$kg\ m^{-3}$]	2770
Specific heat capacity, [$Jkg^{-1}°C^{-1}$]	875
Solidus, [°C]	502
Liquidus, [°C]	638

The FE mesh consisted of 15276 nodes and 12800 elements. The tool and the backing plate are modelled as rigid bodies. Hence, they do not have any thermal degrees of freedom. A simplification is applied to define the geometry of the tool – it does not include the thread, because this would lead to excessive mesh distortion. The model, including the working plate, backing plate, and welding tool, is shown in fig. 2. This figure also provides the main dimensions and movements, as well as two points which are used for determining the development of temperature during the plunge stage, T1 (17.5,0,3) and T2 (12,0,3).

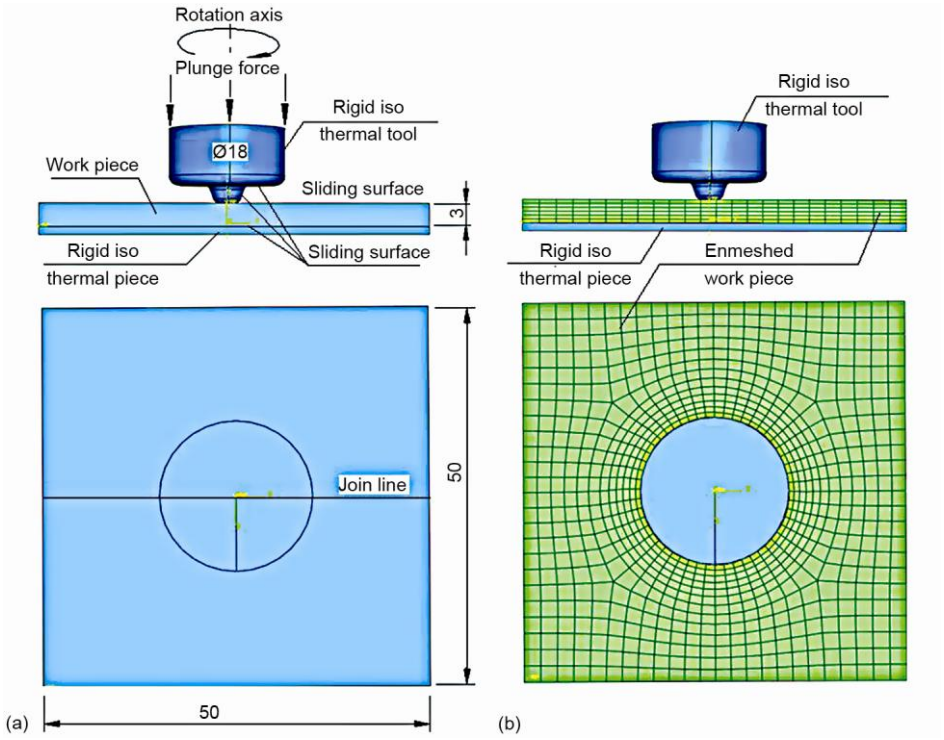

Figure 2. The numerical model (a) and FE mesh (b) – welding plate (work plate), tool, and backing plate

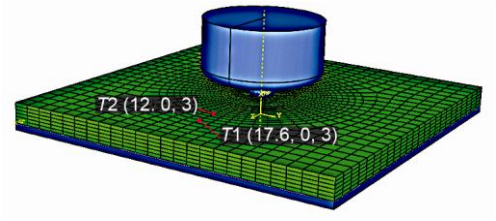

Figure 3. Numerical model with the co-ordinates of the points used for temperature tracking

Johnson-Cook material model

Johnson-Cook model, eq. (1), gives the flow stress of the material depending on temperature, strain and strain rate, [27]. It allows modelling on temperatures up to the melting point or solidus temperature; for the analysed alloys, the solidus temperature is 502 °C, tab. 2.

$$\sigma_y = \left[A + B(\varepsilon_{\mathrm{p}})^n\right]\left[1 + C\left(\frac{\dot{\varepsilon}_{\mathrm{p}}}{\dot{\varepsilon}_o}\right)\right]\left[1 - \left(\frac{T - T_{\mathrm{room}}}{T_{\mathrm{melt}} - T_{\mathrm{room}}}\right)^m\right] \tag{1}$$

where

– for EN AW 2024 T3 alloy, T_{melt} = 502 °C is the melting point or solidus temperature, T_{room} = 25 °C the ambient temperature, T [°C] – the effective temperature, A = 369 MPa the yield stress, B = 684 MPa – the strain factor, n = 0.73 – the strain exponent, m = 1.7 – the temperature exponent, and C = 0.0083 – the strain rate factor;
– for EN AW 2024 T351 alloy, T_{melt} = 502 °C is the melting point or solidus temperature, T_{room} = 25 °C – the ambient temperature, T [°C] – the effective temperature, A = 265 MPa – the yield stress, B = 426 MPa – the strain factor, n = 0.34 – the strain exponent, m = 1 – the temperature exponent, and C = 0.015 – the strain rate factor.

The A, B, C, n, T_{melt} and m are material/test constants for the Johnson-Cook strain rate dependent yield stress for EN AW 2024 T3 and EN AW 2024 T351 [27, 28].

Heat transfer model

During the FSW, two main heat sources exist. The first one is plastic energy dissipation caused by the shear deformation in the welding area (zone). The second one is friction between the tool and the material. A portion of heat generated during welding is conducted into the base material, tool, and the backing plate. The rest is taken away by convection from the surfaces. Certain amount of heat is also lost due to radiation. However, it is assumed to be negligible due to the low temperatures of the FSW process. It can be taken into account together with the convection, by assigning a slightly elevated value of the heat transfer coefficient.

The heat transfer equation can be written:

$$\rho c \frac{\partial T}{\partial t} = \frac{\partial}{\partial x}\left(k_x \frac{\partial T}{\partial x}\right) + \frac{\partial}{\partial y}\left(k_y \frac{\partial T}{\partial y}\right) + \frac{\partial}{\partial z}\left(k_z \frac{\partial T}{\partial z}\right) + \dot{q} \tag{2}$$

where ρ is the density, c – the specific heat, k – the heat conductivity, T – the temperature, t – the time, $\dot{q}$ – the heat generation, and x, y, and z are spatial co-ordinates [29]. The rate of heat generation due to plastic energy dissipation $\dot{q}_p$ is:

$$\dot{q}_{\mathrm{p}} = \eta \tau \dot{\varepsilon}^{\mathrm{pl}} \tag{3}$$

where η is the factor of conversion of mechanical to thermal energy (0.9) [24], τ – the shear stress, and $\dot{\varepsilon}^{\mathrm{pl}}$ is the plastic strain rate. The rate of the heat generation due to the friction between the welding tool and the material can be expressed:

$$\dot{q}_{\mathrm{f}} = \mu p \dot{\gamma} \tag{4}$$

where $\dot{q}_{\mathrm{f}}$ is the frictional heat generation, μ – the coefficient of friction, p – the pressure, and $\dot{\gamma}$ – the slip rate.

The value of the heat transfer coefficient at the bottom surface of the workpiece is 3000 W/m^2°C, [29, 30], this value corresponds to the heat transfer through the backing plate. Heat convection coefficient on the other surfaces of the workpiece are h = 10 W/m^2°C [24, 30]. These surfaces are in the contact with the ambient (air), and the ambient temperature is 25 °C. Friction interaction between the welding tool and the material is characterised by the value of friction coefficient 0.3.

Results and discussion

In order to better understand the temperature differences, diagrams for heat generation due to plastic deformation and friction are first considered, fig. 4. Heat generation due to friction is mostly similar for both alloys. In the 22$^{\mathrm{nd}}$ second, the heat generation for 2024 T3 alloy is lower, due to the less pronounced *squeezing* of the material by the welding tool (higher yield strength, *i. e.* higher resistance to deformation of T3 alloy). Therefore, the contact between the shoulder and the material is established later. Right before the plunge stage is completed, friction heat generation is also slightly lower for 2024 T3 alloy, because the material is heated more intensively. Heat generation due to plastic deformation is more pronounced for this alloy, because of its higher yield strength, *i. e.* the resistance to deformation is higher than in the case of 2024 T351 alloy.

By comparing of the heat generation diagrams with those showing the temperature change (fig. 5), it can clearly be seen that the temperature follows the intensity of heat generation. At the end of the process, 2024 T3 alloy is heated more intensively than 2024 T351 alloy, due to the higher contribution of the heat generation stemming from plastic deformation.

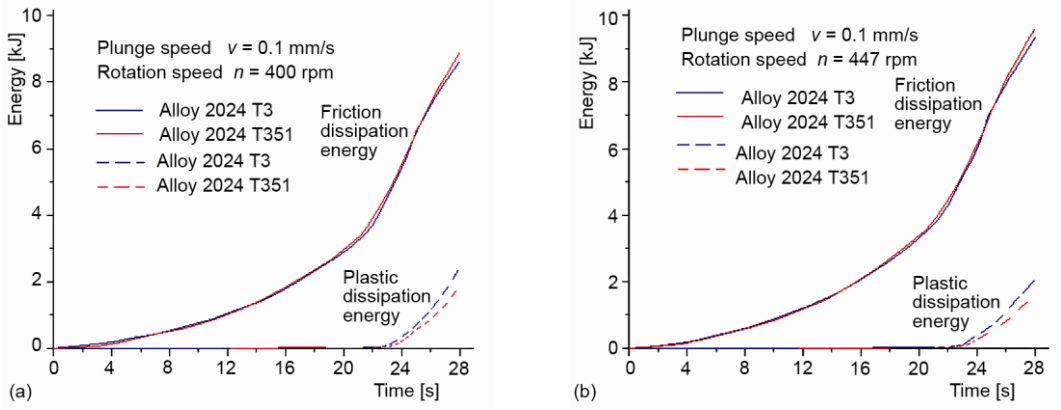

Figure 4. Heat generation for alloys 2024 T3 and 2024 T351; tool plunge speed v_{plunge} = 0.1 mm/s, tool rotation speed n_{rot} = 400 rpm (a), and n_{rot} = 447 rpm (b)

Figure 6 shows temperature distribution on the upper surface of the working plate along the x-axis for both alloys, at the end of the plunge stage. Temperature under the tool shoulder is within the range 430-500 ºC and it is lower for 2024 T351 alloy.

The equivalent plastic strain field at the end of the plunge stage is shown in fig. 7. The values obtained for Al 2024 T351 alloy are higher, due to the more pronounced plasticity

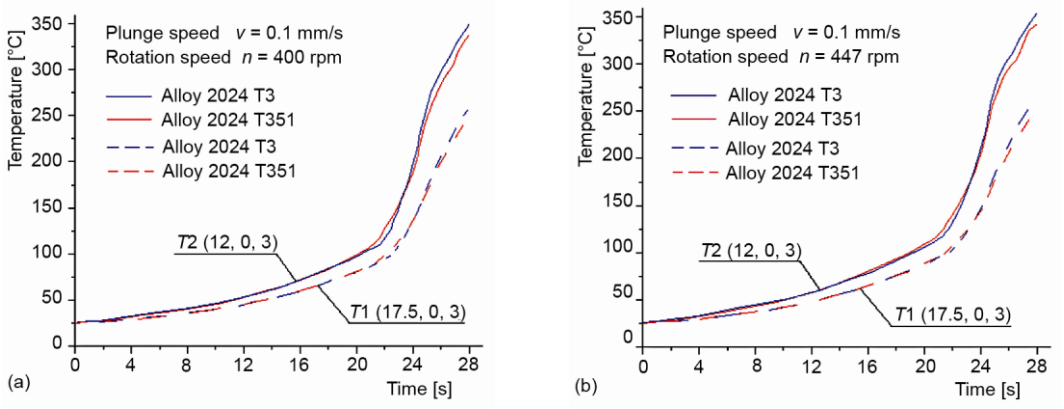

Figure 5. Temperature dependence on time (points T1 and T2), for alloys 2024 T3 and 2024 T351; tool plunge speed v_{plunge} = 0.1 mm/s, tool rotation speed n_{rot} = 400 rpm (a), and n_{rot} = 447 rpm (b)

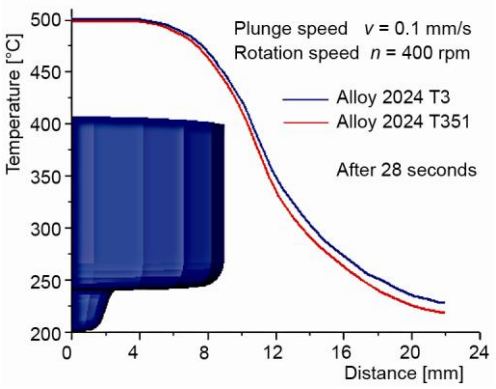

Figure 6. Temperature distribution along the x-axis for alloys 2024 T3 and 2024 T351: tool plunge speed v_{plunge} = 0.1 mm/s, tool rotation speed n_{rot} = 400 rpm

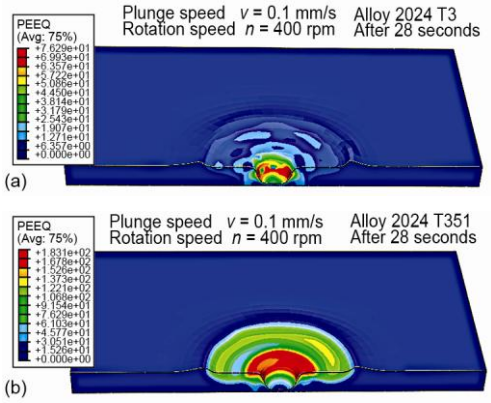

Figure 7. Distribution of equivalent plastic strain after 28 seconds, for alloys 2024 T3 (a) and 2024 T351 (b); tool plunge speed v_{plunge} = 0.1 mm/s, tool rotation speed n_{rot} = 400 rpm

coming from the lower yield strength. For the 2024 T3 alloy, highest equivalent plastic strains are obtained in the zone around the tool pin. If the values under the pin are compared, it can be seen that the equivalent plastic strain is higher for the alloy 2024 T351, and the large strain zone is wider and thicker.

Conclusions

Main conclusions obtained in this study can be summarized:

- The alloy 2024 T3 has more pronounced heat generation from plastic deformation than 2024 T351 alloy, because T3 alloy has higher yield strength and resistance to deformation. Heat generation from friction is only slightly different for the two alloys. Therefore, higher temperatures are obtained for 2024 T3 with the same parameters of the tool plunge.
- Equivalent plastic strain is significantly higher for 2024 T351 alloy than for 2024 T3 alloy, and the values are the highest under the tool shoulder and around the pin basis. For 2024 T3 alloy, equivalent plastic strain is the highest in the influence zone of the tool pin.
- The large strain zone is wider and thicker in the alloy 2024 T351.

- Temperatures of the material in the vicinity of the tool pin are approximately same and their value is around 500 °C.
- Temperature of the material in the welding zone (under the tool shoulder) corresponds to the temperatures of the hot plastic processing (450-500 °C).

Acknowledgment

The authors gratefully acknowledge the support from the Serbian Ministry of Education, Science and Technological Development under the projects TR 34016 and TR 35006.

Nomenclature

A – material parameter of the Johnson-Cook model, [MPa]
A_5 – percentage elongation at fracture, [%]
B – material parameter of the Johnson-Cook model, [MPa]
C – material parameter of the Johnson-Cook model, [–]
c – specific heat capacity, [Jkg^{-1}°C^{-1}]
h – heat convection coefficient, [Wm^{-2}°C^{-1}]
k – thermal conductivity, [Wm^{-1}°C^{-1}]
m – material parameter of the Johnson-Cook model, [–]
n_{rot} – rotation speed of the tool, [rpm]
n – material parameter of the Johnson-Cook model, [–]
p – pressure, [MPa]
$\dot{q}$ – total heat generated, [Js^{-1}]
$\dot{q}_{\mathrm{f}}$ – rate of frictional heat generation, [Js^{-1}]
$\dot{q}_{\mathrm{p}}$ – rate of heat generation due to plastic energy dissipation, [Js^{-1}]
R_m – tensile strength, [MPa]
$R_{p0.2}$ – yield strength, [MPa]
T – temperature, [°C]
T_{melt} – solidus temperature, [°C]
T_{room} – ambient temperature, [°C]
t – time, [s]
v_{plunge} – plunging speed of the tool, [mms^{-1}]
x, y, z – spatial co-ordinates, [m]

Greek symbols

$\dot{\gamma}$ – slip rate [mms^{-1}]
ε_{p} – equivalent plastic strain, [–]
$\dot{\varepsilon}_{\mathrm{p}}$ – equivalent plastic strain rate, [s^{-1}]
$\dot{\varepsilon}_o$ – reference plastic strain rate, [s^{-1}]
η – factor of conversion of mechanical to thermal energy, [–]
μ – coefficient of friction, [–]
ρ – density, [kgm^{-3}]
σ_y – current flow stress in the Johnson-Cook model, [MPa]
τ – shear stress, [MPa]

References

[1] Zhang, H. W., Zhang, Z., Numerical Modeling of Friction Stir Welding Process by Using Rate-dependent Constitutive Model, *Journal of Materials Science & Technology*, *23* (2007), 1, pp. 73-80
[2] Assidi, M., *et al*., Friction Model for Friction Stir Welding Process Simulation: Calibrations from Welding Experiments, *International Journal of Machine Tools & Manufacture*, *50* (2010), 2, pp. 143-155
[3] Eramah, A., *et al.*, Influence of Friction Stir Welding Parameters on Properties of 2024 T3 Aluminum Alloy Joints, *Thermal Science*, *17* (2013), Suppl. 1, pp. S21-S27
[4] Mijajlović, M., *et al.*, Experimental Studies of Parameters Affecting the Heat Generation in Friction Stir Welding Process, *Thermal Science*, *16* (2012), Suppl. 2, pp. S351-S362
[5] Song, M., Kovačević, R., Numerical and Experimental Study of the Heat Transfer Process in Friction Stir Welding, *Journal of Engineering Manufacture*, *217* (2003), 1, pp. 73-85
[6] Chen, C. M., Kovačević, R., Finite Element Modelling of Friction Stir Welding – Thermal and Thermomechanical Analysis, *International Journal of Machine Tools & Manufacture*, *43* (2003), 13, pp. 1319-1326
[7] Al-Badour, F., *et al.*, Thermo-Mechanical Finite Element Model of Friction Stir Welding of Dissimilar Alloys, *International Journal of Advanced Manufacturing Technology*, *72* (2014), 5-8, pp. 607-617
[8] Dong, P., *et al.*, Coupled Thermomechanical Analysis of Friction Stir Welding Process Using Simplified Models, *Science and Technology of Welding and Joining*, *6* (2001), 5, pp. 281-287
[9] He, X., *et al.*, A Review of Numerical Analysis of Friction Stir Welding, *Progress in Materials Science*, *65* (2014), Aug., pp. 1-66
[10] Veljić, D., *et al.*, Numerical Simulation of the Plunge Stage in Friction Stir Welding, *Structural Integrity and Life*, *11* (2011), 2, pp. 131-134

[11] Veljić, D., *et al.*, A Coupled Thermo-Mechanical Model of Friction Stir Welding, *Thermal Science, 16* (2012), 2, pp. 527-534
[12] Veljić, D., *et al.*, Heat Generation during Plunge Stage in Friction Stir Welding, *Thermal Science, 17* (2013), 2, pp. 489-496
[13] Kim, D., *et al.*, Numerical Simulation of Friction Stir Butt Welding Process for AA5083-H18 Sheets, *European Journal of Mechanics A/Solids, 29* (2010), 2, pp. 204-215
[14] Feulvarch, E., *et al.*, A Simple and Robust Moving Mesh Technique for the Finite Element Simulation of Friction Stir Welding, *Journal of Computational and Applied Mathematics*, *246* (2013), July, pp. 269-277
[15] Perović, M., *et al.*, Friction-Stir Welding of High-Strength Aluminum Alloys and a Numerical Simulation of the Plunge Stage, *Materials and Technologies, 46* (2012), 3, pp. 105-111
[16] Eramah, A., *et al.*, Impact Fracture Response of Friction Stir Welded Al-Mg Alloy, *Structural Integrity and Life, 13* (2013), 3, pp. 171-177
[17] ***, Certificate Conformity, ALCOA International, Inc, Approved Certificate No. 47831, 1990
[18] ***, ASM International Aluminum 2024-T3 Data Sheet, http://asm.matweb.com/search/SpecificMaterial.asp?bassnum = MA2024T3
[19] Ivanović, I., *et al.*, Numerical Study of Transient Three-Dimensional Heat Conduction Problem with a Moving Heat Source, *Thermal Science, 15* (2011), 1, pp. 257-266
[20] Berković, M., *et al.*, Analysis of Welded Joints by Applying the Finite Element Method, *Structural Integrity and Life, 4* (2004), 2, pp. 75-83
[21] Aburuga, T., *et al.*, Numerical Aspects for Efficient Welding Computational Mechanics, *Thermal Science, 18* (2014), Suppl. 1, pp. S139-S148
[22] Živojinović, D., *et al.*, Crack Growth Analysis in Friction Stir Welded Joint Zones Using Extended Finite Element Method, *Structural Integrity and Life, 13* (2013), 3, pp. 179-188
[23] ***, Dassault Systemes, Abaqus Analysis Manual, 2014
[24] Schmidt, H., Hattel, J., A Local Model for the Thermomechanical Conditions in Friction Stir Welding, *Modelling & Simulation in Materials Science and Engineering, 13* (2005), 1, pp. 77-93
[25] Zhang, Z., *et al.*, Effect of Traverse/Rotational Speed on Material Deformations and Temperature Distributions in Friction Stir Welding, *Journal of Materials Science & Technology, 24* (2008), 6, pp. 907-913
[26] Veljić, D., *et al.*, Thermo-Mechanical Modelling of Friction Stir Welding, *Proceedings*, 4th International Conference on Innovative Technologies for Joining Advanced Materials, Timisoara, Romania, 2010, pp. 171-176
[27] Johnson, G. R., Cook, W. H., A Constitutive Model and Data for Metals Subjected to Large Strains, High Strain Rates and High Temperatures, *Proceedings*, 7th International Symposium on Ballistics, The Hague, The Netherlands, 1983, pp. 541-547
[28] Lesuer, D. R., Experimental Investigations of Material Models for Ti-6Al-4V Titanium and 2024-T3 Aluminum, Final Report, Department of Transportation, Washington DC, USA, 2000
[29] Park, K., Development and Analysis of Ultrasonic Assisted Friction Stir Welding Process, Ph. D. thesis, University of Michigan, Ann Arbor, Mich., USA, 2009
[30] Veljić, D., *et al.*, Experimental and Numerical Thermo-Mechanical Analysis of Friction Stir Welding of High-Strength Aluminum Alloy, *Thermal Science, 17* (2013), Suppl. 1, pp. S28-S37

Paper submitted: March 13, 2015
Paper revised: April 20, 2015
Paper accepted: April 20, 2015